Foldings and grazings of tori in current controlled interleaved boost converters

Damian Giaouris[1,*,†], Soumitro Banerjee[2,3], Fotis Stergiopoulos[4],
Simira Papadopoulou[4], Spyros Voutetakis[1], Bashar Zahawi[5], Volker Pickert[5],
Abdullah Abusorrah[6], Mohammed Al Hindawi[6] and Yusuf Al-Turki[6],

[1]*Chemical Process Engineering Research Institute (C.P.E.R.I.), Centre for Research and Technology Hellas (CE.R.T.H.)*
57001 Thermi-Thessaloniki, Greece
[2]*Indian Institute of Science Education and Research, Nadia, 741252 WB India*
[3]*King Abdulaziz University, Jeddah, Saudi Arabia*
[4]*Department of Automation, Alexander Technological Educational Institute of Thessaloniki, Thessaloniki, Greece*
[5]*School of Electrical and Electronic Engineering, Newcastle University, England, UK*
[6]*Electrical and Computer Engineering Department, Faculty of Engineering, King Abdulaziz University, Jeddah, Saudi Arabia*

SUMMARY

Interleaved boost converters (IBCs) are used when energy conversion is required at high current levels. Such converter systems may undergo various nonlinear phenomena which can affect their performance adversely. In this paper, we study an IBC and demonstrate the first instability through a Neimark–Sacker bifurcation, resulting in a torus. An analysis based on the calculation of the monodromy matrix reveals that the torus has a rather strange form as the complex Floquet multipliers that became unstable have a real value close to −1. We show that further variation in a parameter can result in novel nonlinear phenomena where the torus itself folds and grazes a switching manifold, resulting in a 'wobbling' of the closed loop that represents the torus in discrete time. Numerical and analytical results validate our work. Copyright © 2013 John Wiley & Sons, Ltd.

1. INTRODUCTION

Power converters have to be connected in parallel whenever power conversion is necessary at a higher value of current than what the devices can carry [1–6]. By paralleling converters, the inductor current in each phase is reduced, and hence the size of the inductor can be decreased [1,7–10]. This may be necessary in high-current applications like motor drives and battery chargers, and also in situations where the current carrying capacity of the switch is small, as is the case in on-chip power converters.

As with single converters, it is possible to control the voltage and/or the current depending on the application [11–14]. In electric drives, usually an inner current loop and an outer voltage loop are required, while in battery chargers, only a current loop is often employed.

Various strategies for controlling parallel-connected converters have been proposed in the literature and are used in industry. These include, among others, the Master–slave logic [15, 16] and the Winner-Take-All logic [17]. It is usually desired in parallel converters that the switches in the different legs

---

*Correspondence to: Damian Giaouris, Chemical Process Engineering Research Institute (C.P.E.R.I.), Centre for Research and Technology Hellas (CE.R.T.H.), P.O. Box 60361, 57001 Thermi-Thessaloniki, Greece.
†E-mail: damian.giaouris@ncl.ac.uk, giaouris@cperi.certh.gr

operate in a complementary fashion (interleaving operation) thus reducing the current ripples seen by the source and the load. The aforementioned strategies may be used for interleaving operation [15], for example by appropriately designing the triangular waveforms used to produce the PWM signals. Another approach is to directly control the switches complementarily [18] by normal peak current controllers whose clock signals have an appropriate phase delay. It is also possible to have only one peak current controller for the first phase and then to appropriately delay and use the delayed control signal for the other phases. Like conventional dc-dc converters [19–29], parallel connected converters may also undergo various bifurcations that force the converter to operate in an undesirable way [30–32, 18,17,10]. This can cause many problems to the converter as it can increase the current/voltage ripple, add extra harmonics and increase the switching losses. It has been demonstrated [23] that it is possible for parallel-connected buck converters to lose stability either through a period doubling bifurcation or through a slow-scale bifurcation [15], while parallel-connected boost converters go through a slow-scale (Neimark–Sacker) bifurcation. Some work has been done in studying the evolution of the torus in dc-dc converters [33–36], and how it may be deformed or even destroyed. Normally, the mechanism involves a homoclinic intersection between the stable and unstable manifolds of a saddle fixed point. In this paper, we demonstrate a new mechanism of deformation of the torus through interaction with a switching manifold.

We study a two-phase interleaved boost converter (IBC) with two peak current controllers (one for each phase). We report for the first time four interesting phenomena: (1) that a torus is created through a slow-scale bifurcation of a fixed point with complex eigenvalues that have real part close to −1, and hence the bifurcation has some characteristics of period doubling, (2) a folding that occurs on the torus when the duty cycle becomes greater than 0.5, (3) a wobbling that appears on the torus when it grazes one of the switching manifolds and (4) a saddle-node bifurcation on the torus creating a period-4 orbit.

2. SYSTEM DESCRIPTION

The IBC has multiple 'legs' with inductors and switches sharing a common output capacitor. The input current is distributed among the parallel legs which turn on sequentially, so that the input current ripple is kept low and smaller inductances/diodes can be used. A simple approach to control these converters is to use a peak current controller for the first leg and then delay the control signal by $2\pi/n$ for the other phases, where n is the number of the corresponding phase. Mathematically, this creates a piecewise smooth vector field with one switching manifold that depends on the state vector and n-1 manifolds that depend only on time. However, this approach does not allow independent control of the separate legs which may be necessary at times to meet the demanded current. In such cases, n separate controllers are used for each phase, whose clock signals are separated by $2\pi/n$. This ensures the proper and safe operation of each phase even in the case of unbalanced operation. In this work, a two-leg converter was chosen for simplicity (Figure 1), and two separate controllers for the two phases were used.
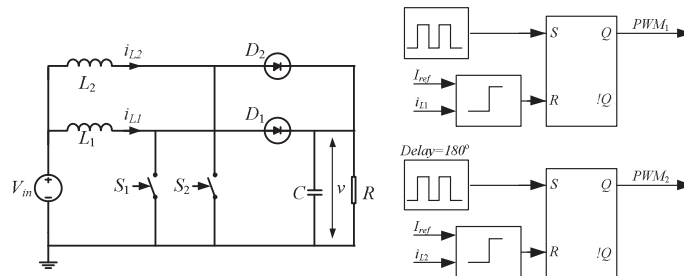

Figure 1. Schematic diagram of the current controlled interleaved boost converter. The nominal parameter values taken in this study are $V_{\text{in}} = 5$ V, $R = 40$ Ω, $L = 1.5$ mH, $C = 10$ μF, $T = 100$ μs.

The mathematical model of the system is given by the state space equations:

$$\frac{d}{dt}\begin{bmatrix} v \\ i_{L_1} \\ i_{L_2} \end{bmatrix} = \begin{bmatrix} -1/RC & \bar{s}_1/C & \bar{s}_2/C \\ -\bar{s}_1/L & 0 & 0 \\ -\bar{s}_2/L & 0 & 0 \end{bmatrix}\begin{bmatrix} v \\ i_{L_1} \\ i_{L_2} \end{bmatrix} + \begin{bmatrix} 0 \\ \dfrac{V_{in}}{L} \\ \dfrac{V_{in}}{L} \end{bmatrix} \tag{1}$$

where $\bar{s}_i = 1$ when the switch S_i is OFF. The two switching manifolds are given by $h_1(x,t) = x_2 - I_{ref}$, $h_2(x,t) = x_3 - I_{ref}$. The orbit is allowed to move in the state space inside the area confined by these two fixed switching borders, but cannot cross them. In order to obtain a Poincaré map, the state vector has to be sampled in synchronism with the clock of *one* of the legs (we choose that of the first leg). As the system is symmetrical, this will not cause a problem. However, this aspect has to be kept in mind when analyzing the orbit, especially when the legs are unbalanced.

When the demanded current in each phase is 0.1 A, the response is a normal period-1 orbit as shown in Figure 2. The current in the second leg is delayed by $T/2$s from that of the first leg, and the system goes through the following sequence of switch states: (1) where S_1 is ON and S_2 is OFF, (2) where S_1 and S_2 are OFF, (3) where S_1 is OFF and S_2 is ON and (4) where S_1 and S_2 are OFF. The duty ratio is given by $d = T_{on}/T$, where T_{on} is the time that the switch is closed during one clock period.

As the demanded current is increased, this orbit loses stability through a slow-scale bifurcation as expected, [23]. In this particular case, the resulting orbit has rather strange characteristics, as shown in Figure 3(a). As I_{ref} changes from 0.291165 A to 0.291167 A, the stable periodic orbit develops a slow sinusoidal oscillation. However, the samples on the torus jump from one side to the other as can be seen in Figure 3(a).
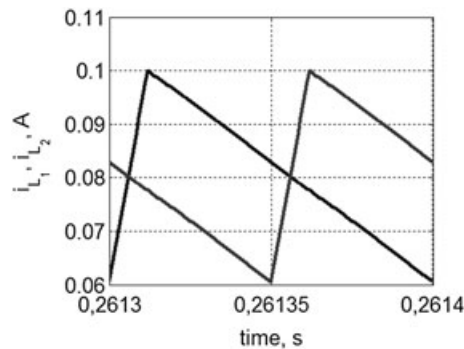

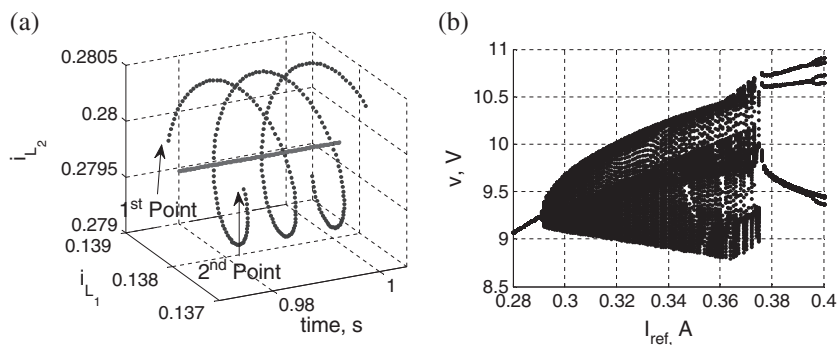Figure 2. Time response of the two currents for $I_{ref} = 0.1$ A.

Figure 3. (a) Sampled time response showing the unstable period-1 point and the stable torus at $I_{ref} = 0.291167$ A. (b) Bifurcation diagram of a two-leg interleaved converter under peak current control.

3. STABILITY ANALYSIS OF THE PERIOD-1 ORBIT

In order to study the aforementioned bifurcation, the eigenvalues of the fixed point in the Poincaré map were calculated. As shown in [37], it is possible to determine the stability of the orbit by calculating the monodromy matrix of the limit cycle (the state transition matrix over a complete clock period). Care must be taken to include the effect of the two switching instances using the saltation matrix, [38, 39], see also the analysis in the appendix. The duty cycle can be calculated using the methodology presented in [37] or, assuming equal inductances, using the formula:

$$I_{ref} = \frac{V_{in}}{2} \left(\frac{1}{R(1-D)^2} + \frac{DT}{L} \right) \qquad (2)$$

where D is the steady-state duty cycle. The eigenvalues of the period-1 limit cycle for different values of I_{ref} are given in Table I which clearly show a Neimark–Sacker or slow-scale bifurcation [40] at $I_{ref}=0.291166$ A. The resulting birth of a torus is confirmed by the bifurcation diagram of Figure 3(b). It is interesting to highlight the fact that at this bifurcation, the real part of the complex eigenvalues also is close to -1, and hence the bifurcation has the dual characteristics of period doubling as well as a Neimark–Sacker bifurcation. Because of the period doubling, a period-2 point develops on the Poincaré section, and because of the (small) imaginary part, the two points rotate on a closed loop. Close to the bifurcation point, the angle between two successive points on the torus is $tan^{-1}0.0349/-0.9994=3.1066$ rads which agrees with our observation that the points on the torus jump from one side to another (Figure 3(a)).

In an earlier publication, the occurrence of an 'interactive bifurcation' was reported [41], where a pair of complex conjugate eigenvalues goes out of the unit circle, and at the same time a real eigenvalue crosses -1. In contrast, a single pair of complex eigenvalues crossed the unit circle, but had the real part close to -1 in the bifurcation described in this paper. Furthermore, two-dimensional bifurcation diagrams were produced in order to check if this were a co-dimension 2 bifurcation or a case of 1:2 strong resonance [40]. The bifurcation parameters were chosen to be the supply voltage, V_{in}, and the demanded current, I_{ref}. In all cases, the period-1 orbit lost stability through a slow-scale bifurcation with a real eigenvalue close to -1. This excludes the possibility of having a 1:2 strong resonance. To our knowledge, such a bifurcation has not been reported earlier in power electronic systems.

Table I. Floquet multipliers.

I_{ref}	d	x_0	Eigenvalues	Magnitude
0.1	0.1184	$\begin{bmatrix} 5.6977 \\ 0.0605 \\ 0.0829 \end{bmatrix}$	$\begin{bmatrix} 0.3132 \\ -0.1949 \pm 0.0014i \end{bmatrix}$	$\begin{bmatrix} 0.3132 \\ 0.1972 \end{bmatrix}$
0.25	0.4367	$\begin{bmatrix} 8.5512 \\ 0.1125 \\ 0.2296 \end{bmatrix}$	$\begin{bmatrix} 0.5255 \\ -0.8324 \pm 0.0125i \end{bmatrix}$	$\begin{bmatrix} 0.5255 \\ 0.8325 \end{bmatrix}$
0.29	0.4587	$\begin{bmatrix} 9.2360 \\ 0.1371 \\ 0.2784 \end{bmatrix}$	$\begin{bmatrix} 0.5428 \\ -0.9947 \pm 0.0341i \end{bmatrix}$	$\begin{bmatrix} 0.5428 \\ 0.9953 \end{bmatrix}$
0.291166	0.4599	$\begin{bmatrix} 9.2553 \\ 0.1379 \\ 0.2799 \end{bmatrix}$	$\begin{bmatrix} 0.5432 \\ -0.9994 \pm 0.0349i \end{bmatrix}$	$\begin{bmatrix} 0.5432 \\ 1 \end{bmatrix}$
0.3	0.4690	$\begin{bmatrix} 9.4006 \\ 0.1437 \\ 0.2910 \end{bmatrix}$	$\begin{bmatrix} 0.5462 \\ -1.0346 \pm 0.0408i \end{bmatrix}$	$\begin{bmatrix} 0.5462 \\ 1.0354 \end{bmatrix}$

4. FOLDING OF THE TORUS

As the demanded current is further increased, we observe a folding in the torus as shown in Figure 4(a).

In order to understand why this folding occurs, we need to consider the behavior of a period-1 orbit for various values of the duty cycle. Generally, it is possible to have three qualitatively different responses, shown in Figure 5. In the first case ($D < 0.5$), the first phase is ahead of the second, and the switching modes are: (ON, OFF) $\rightarrow$ (OFF, OFF) $\rightarrow$ (OFF, ON) $\rightarrow$ (OFF, OFF). When $D = 0.5$, we have only two cases: (ON, OFF) $\rightarrow$ (OFF, ON), while when $D > 0.5$, the switching modes are: (ON, ON) $\rightarrow$ (ON, OFF) $\rightarrow$ (ON, ON) $\rightarrow$ (OFF, ON). Hence, we have a border collision (change in topological sequence) when the duty cycle becomes 0.5.

When the torus develops in the system under consideration, the duty ratio varies from cycle to cycle. When the demanded current becomes 0.29154 A, there are cycles on the torus that have duty ratio greater than 0.5. Numerical simulations showed that the maximum value of the duty cycle is 0.5005, and that causes the onset of folding. By further increasing the demanded current, the folding becomes more severe. Furthermore, as can be seen from Figure 6, the folding happens exactly where the torus touches the demanded current (0.3 A here). This can be explained by Figure 5. For $D = 0.5$ at $t = 0$ (the sampling instant), the current in the second phase is equal to I_{ref} (Figure 5(b)). As the
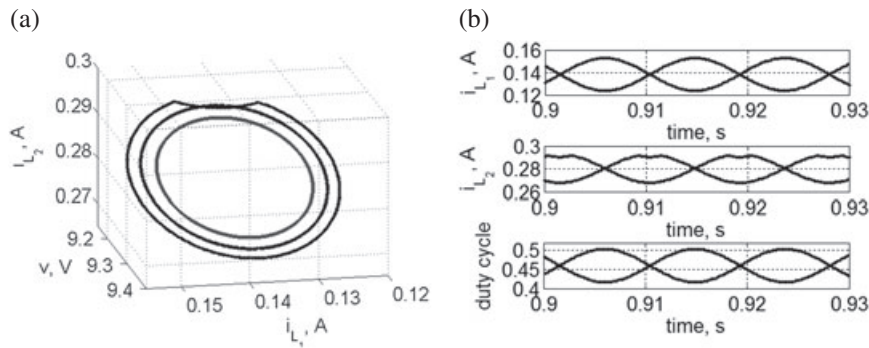

Figure 4. (a) Sampled state space orbit showing the folding, inner cycle for $I_{ref} = 0.2915$ A, middle cycle for $I_{ref} = 0.29152$ A, outer cycle for $I_{ref} = 0.2916$ A. (b) Time domain waveforms of the sampled currents and duty cycle of the first leg for $I_{ref} = 0.2916$ A.
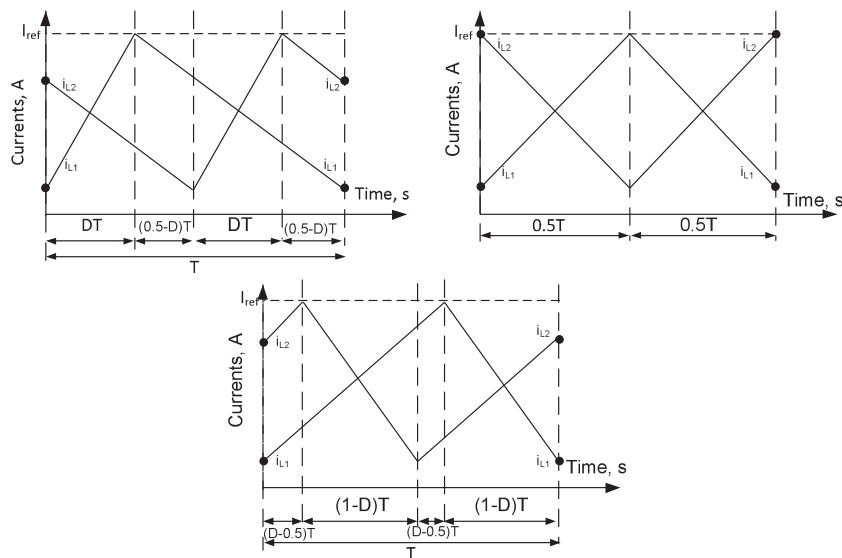

Figure 5. Typical waveforms for $D < 0.5, D = 0.5, D > 0.5$.
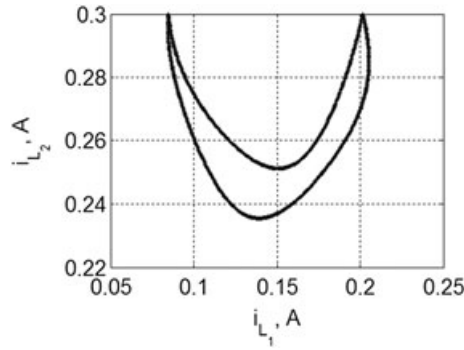
Figure 6. 2D sampled state space showing the folding, $I_{ref} = 0.3$ A.

demanded current is increased and $D > 0.5$ (Figure 5(c)), the current at the observation instant will be less than I_{ref} (Figure 4b). This folding also stops the expansion of the torus as seen in Figure 3(b).

5. GRAZING OF THE TORUS

Another interesting phenomenon occurs when the demanded current is further increased; the torus goes through repeated foldings much like the 'chattering' problem of mechanics (but unlike chattering this happens in discrete time). The bifurcation diagram of Figure 3(b) shows some change in the structure at around $I_{ref} = 0.36$ A. Figure 7 shows the torus when $I_{ref} = 0.365$ A where we see a deformation of the loop. Following the sequence of events that leads to it, we find that this repeated folding is caused by the grazing of the torus with the switching manifold. Figure 8 clearly shows that when $I_{ref} = 0.35$ A, the torus is away from the manifold and when $I_{ref} = 0.36$ A, it just grazes it, which initiates the repeated folding or 'wobbling'.

Note that the grazing of the torus with the switching surface occurs in discrete time. Such a phenomenon has earlier been reported in a mechanical system [42]. Furthermore, it is interesting to note that even though the grazing occurs only in the area around $i_{L_1} = I_{ref}$, the deformation is observed in four different regions of the closed loop (Figure 7). This is explained by the facts that (1) the fixed point located inside the closed loop has eigenvalues close to -1 and (2) there is a symmetry between the two states. As it has been mentioned, when the orbit grazes the switching manifold, multiple foldings take place that force the torus to deform. Due to the negative eigenvalue, the points on the sampled torus jump from right to left and vice versa (see Figure 3(a)), and hence this wobbling also appears on the left of the torus in the area where $i_{L_1} \simeq 0.05$ A. Also, there is a symmetry between the two phases, and hence whatever happens in one phase in one specific instant
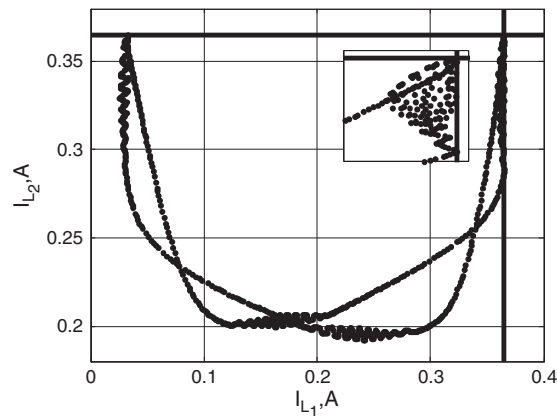

Figure 7. Sampled 2D torus when $I_{ref} = 0.365$ A, including the two switching manifolds.
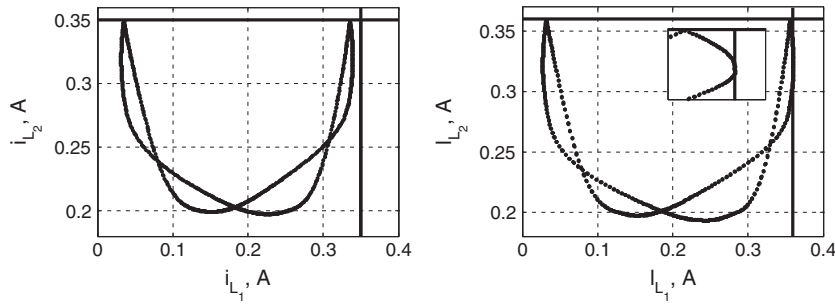
Figure 8. Sampled 2D torus at $I_{ref} = 0.35$ A and 0.36 A, including the two switching manifolds, showing the onset of grazing.

will also happen in the other phase after a lapse of $T/2$s. When the period-1 orbit lost stability through a slow-scale bifurcation, the torus that was created inherited this property. Suppose, starting from any point on the torus, one has to go through N iterates to traverse the loop. Because of the above symmetry, whatever happens on the torus at one specific point will also appear after $N/2$ samples [43]. In this case, one has to go through approximately 138 iterates to traverse the loop, and hence the wobbling appears again after 69 samples. This explains the two areas where the wobbling appears in the bottom of the torus $i_{L_2} \simeq 0.2\ A$. In order to further validate this, three- and four-legged converters were simulated, which showed that indeed the deformation appears after N/n points on the torus, where n is the total number of phases.

6. SADDLE-NODE BIFURCATION

After the onset of wobbling, as the demanded current is further increased, the wobbling increases, and the torus appears to have rings on it (Figure 9), as if locally, there are period doublings on the torus. This is revealed to be the approach of an impending saddle-node bifurcation. In the run-up to the bifurcation, the round-trip time around the loop increases as a 'bottleneck' develops, and the period increases to infinity. In many features, this is similar to the infinite period bifurcation observed in continuous-time systems [44]: (1) that there is a bottleneck on the torus, i.e. points gather in specific areas on the limit cycle in the sampled state space, (2) that the round-trip time around the closed loop increases to infinity following an inverse square root law: $T \propto 1/\sqrt{|I_{ref_{bif}} - I_{ref}|}$ and (3) that the torus is destroyed by a saddle-node bifurcation, i.e. a stable and an unstable limit cycle are created with one eigenvalue being 1.

After the onset of rings at $I_{ref} = 0.375$, we observe that more points of the torus are gathered around these rings. This is clear when Figure 8 is compared with Figure 9. The two figures are plotted with the same number of points, but in Figure 9, a large number of points accumulate on the rings while the other parts of the torus are sparsely populated. The rings, thus, represent the bottlenecks.
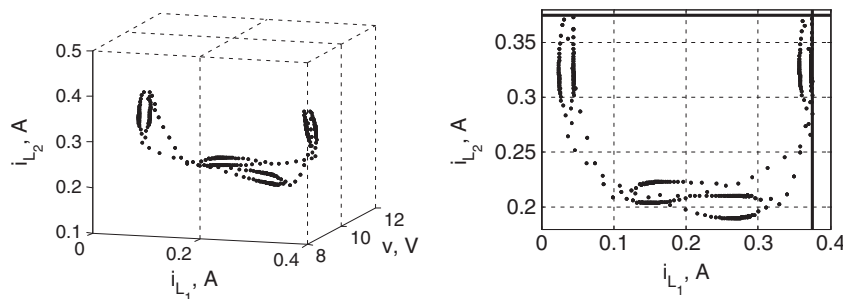

Figure 9. 3D and projected 2D sampled state space when $I_{ref} = 0.375$ A, including the two switching manifolds.

Furthermore, as we increase the demanded current, we see that the time taken to traverse the closed loop also increases [43]. For example, when $I_{ref} = 0.375$ A, we need approximately 337 samples (or 0.0337s) to complete a circle, while for 0.376 A we need 707 samples. Figure 10 shows that the round-trip time becomes infinite at around $I_{ref} = 0.3762718$ A obeying an inverse square root law. In order to check the character of the period-4 orbit that appears towards the right of Figure 3(b), we used a method similar to that in [43] and calculated the eigenvalues as the parameter is decreased toward the bifurcation point; see also the analysis in the appendix. It was revealed that the period-4 orbit has an eigenvalue of 1 just after the bifurcation point (Table II), which indicates the occurrence of a saddle-node bifurcation.

7. CONCLUSION

In this paper, we reported an instability in the IBC that is a Neimark–Sacker bifurcation with some features of period doubling. In this bifurcation, a pair of complex eigenvalues crosses the unit circle with real part close to -1 (i.e. the imaginary part is very small compared to the real part). This bifurcation causes the Poincaré section points to flip between the opposite ends of a closed loop, and to rotate on the closed loop.

We have also shown that the torus undergoes a fold when it makes contact with the switching manifold. Further contacts with the switching manifold causes repeated foldings in quick succession, which appear in ring-like structures on the closed loop. This is a grazing induced bifurcation where the discrete-time closed loop grazes the switching manifold. Finally, we show that the torus is destroyed by a saddle-node bifurcation.

APPENDIX A

In this section, we present the detailed steps in calculating the eigenvalues of the period-1 orbit in Section 3 and of the period-4 orbit in Section 4.
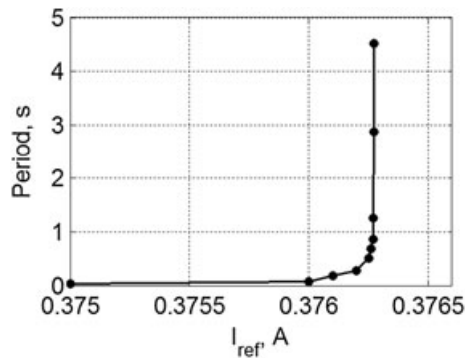

Figure 10. The number of iterates in one full rotation around the torus versus demanded current showing that the round-trip time increases to infinity.

Table II. Floquet multipliers of the period-4 orbit.

I_{ref}	Eigenvalues
0.37700	0.8777, 0.1847, $-$ 0.8358
0.37680	0.8968, 0.1818, $-$ 0.8325
0.37650	0.9333, 0.1765, $-$ 0.8262
0.37640	0.9503, 0.1742, $-$ 0.8235
0.37635	0.9614, 0.1728, $-$ 0.8218
0.37632	0.9697, 0.1717, $-$ 0.8205
0.37630	0.9769, 0.1709, $-$ 0.8195

Eigenvalues of the period-1 orbit before the slow-scale bifurcation

According to (1), Figures 5 and 11, for $D < 0.5$ (a similar analysis can be followed for $D > 0.5$), the evolution of the orbit in the state space is being governed by the following equations:

$$x(DT) = e^{A(s_i)DT}x_0 + \int_0^{DT} e^{A(s_i)(DT-\tau)}Rd\tau = \Phi_1 x_0 + I_1$$

$$x(0.5T) = e^{A(s_i)(0.5-D)T}x(DT) + \int_{DT}^{0.5T} e^{A(s_i)(0.5T-\tau)}Rd\tau = \Phi_2 x(DT) + I_2$$

$$x((0.5+D)T) = e^{A(s_i)DT}x(0.5T) + \int_{0.5T}^{(0.5+D)T} e^{A(s_i)((0.5+D)T-\tau)}Rd\tau = \Phi_3 x(0.5T) + I_3$$

$$x(T) = e^{A(s_i)(0.5-D)T}x((0.5+D)T) + \int_{(0.5+D)T}^{T} e^{A(s_i)(T-\tau)}Rd\tau = \Phi_4 x((0.5+D)T) + I_4$$

where $R = \begin{bmatrix} 0 & V_{in}/L & V_{in}/L \end{bmatrix}^T$. The state transition matrices Φ are calculated using a series expansion:

$$\Phi = e^{At} = \sum_{i=0}^{\infty} (At)^i / i \tag{3}$$

In this work, the series was expanded up to seventh-order components.

Combining the above equations, we have the following expression that allows us to calculate the location of the limit cycle using (2):

$$x(T) = x_0 = \Phi_4(\Phi_3(\Phi_2(\Phi_1 x_0 + I_1) + I_2) + I_3) + I_4 \tag{4}$$

From Figure 11, we see that the period-1 orbit has two switching events that need to be represented by a saltation matrix, one at $t = DT$ and one at $t = (0.5+D)T$; hence, the Monodromy matrix is given by [37]:

$$\Phi(T, 0, x(0)) = \Phi_4 \times S_2 \times \Phi_3 \times \Phi_2 \times S_1 \times \Phi_1 \tag{5}$$

where the saltation matrices are given by:

$$S = I + \frac{(f_- - f_+)n^T}{n^T f_+ + \frac{\partial h}{\partial t}|_{t=t_\Sigma}} \tag{6}$$

Therefore, for each value of the demanded current, we use (2) to find the duty cycle and then (4) to find the location of the limit cycle and hence the switching instants and points. The state transition
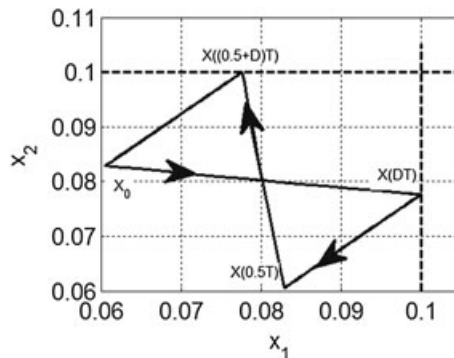

Figure 11. State space for $I_{ref} = 0.1$ A.

matrices are calculated by (3), and then with (5) and (6), we can find the Floquet multipliers and hence can determine the stability of the system.

For example, for $I_{ref} = 0.2$ A, (2) gave a duty cycle of $D = 0.3397$, and from (4) $x(0) = \begin{bmatrix} 7.6397 & 0.0868 & 0.1726 \end{bmatrix}^T$. The 4 state transition matrices are:

$$\Phi_4 = \Phi_2 = \begin{bmatrix} 0.9441 & 1.5618 & 1.5618 \\ -0.0104 & 0.9916 & -0.0084 \\ -0.0104 & -0.0084 & 0.9916 \end{bmatrix}, \Phi_3 = \Phi_1 = \begin{bmatrix} 0.8824 & 3.2157 & 0 \\ -0.0214 & 0.9628 & 0 \\ 0 & 0 & 1 \end{bmatrix}$$

The two saltation matrices are:

$$S_1 = \begin{bmatrix} 1 & 6.0033 & 0 \\ 0 & -0.4965 & 0 \\ 0 & 0 & 1 \end{bmatrix}, S_2 = \begin{bmatrix} 1 & 0 & 6.0033 \\ 0 & 1 & 0 \\ 0 & 0 & -0.4965 \end{bmatrix}$$

This gives the monodromy matrix as:

$$\Phi(T, 0, x(0)) = \begin{bmatrix} 0.4496 & 1.1078 & 7.9482 \\ -0.0309 & -0.6567 & -0.2303 \\ 0.0101 & 0.0114 & -0.5503 \end{bmatrix}$$

And therefore the Floquet multipliers are:

$$\begin{bmatrix} 0.4920 & -0.6247 + 0.0013i & 0.6247 - 0.0013i \end{bmatrix}^T$$

Eigenvalues of the period-4 orbit after the torus destruction

In order to determine the stability of the period 4, we calculated the eigenvalues of the stable period-4 orbit just before it lost stability, going from higher to lower values of I_{ref}. For each value of I_{ref}, we find the stable period-4 orbit by simulating the system until it reaches a stable behavior. The state variables at the beginning of the period are extracted from it. For example, at $I_{ref} = 0.3763$ A, these values are $x_0 = \begin{bmatrix} 9.8216 & 0.2758 & 0.2122 \end{bmatrix}^T$.

Then, we add a small perturbation to x_0, and we record the value of $x(4T)$. Since there are nine unknown variables (the elements of the monodromy matrix), we repeat the same process two more times. Thus, we have nine equations with nine unknowns which can easily be solved to determine the elements of the monodromy matrix. Specifically, for the aforementioned value of I_{ref} we used three different initial conditions:

$$x_A(0) = \begin{bmatrix} x_0(1) \times 0.9999 \\ x_0(2) \times 1.0001 \\ x_0(3) \times 1.0001 \end{bmatrix}, x_B(0) = \begin{bmatrix} x_0(1) \times 1.0001 \\ x_0(2) \times 1.0001 \\ x_0(3) \times 0.99998 \end{bmatrix}, x_C(0) = \begin{bmatrix} x_0(1) \times 0.9999 \\ x_0(2) \times 1.0001 \\ x_0(3) \times 0.9999 \end{bmatrix}$$

Simulations starting from these initial conditions gave three state vectors at $t = 4T$. Substituting in the equation

$$x(4T) = \Phi(4T, 0, x(0))x(0),$$

we get nine equations with nine unknowns, which when solved gave the monodromy matrix:

$$\begin{bmatrix} -0.1427 & -8.9559 & -0.9714 \\ 0.0318 & 1.2320 & 0.2985 \\ 0.0390 & 0.3062 & -0.7610 \end{bmatrix}$$

with the eigenvalues:

$$\begin{bmatrix} 0.9769 & 0.1709 & -0.8195 \end{bmatrix}^T$$

This process was repeated for all values of I_{ref} that appear in section 6.

REFERENCES

1. Huang Y, Tse CK. Circuit theory of paralleling switching converters. *International Journal of Circuit Theory and Applications* 2009; **37**(1):109–135.
2. Thounthong P, Pierfederici S. A new control law based on the differential flatness principle for multiphase interleaved dc-dc converter. *IEEE Transactions on Circuits and Systems-II* 2010; **57**(11):903–907.
3. Lin B, Huang C, Li M. Novel interleaved zvs converter with ripple current cancellation. *International Journal of Circuit Theory and Applications* 2009; **37**(3):413–431.
4. Veerachary M, Senjyu T, Uezato K. Signal flow graph modelling of interleaved buck converters. *International Journal of Circuit Theory and Applications* 2003; **31**(3):249–264.
5. Veerachary M, Senjyu T, Uezato K. Small-signal analysis of interleaved dual boost converter. *International Journal of Circuit Theory and Applications* 2001; **29**(6):575–589.
6. Lin BR, Chao CH, Chiang YJ. Implementation of an interleaved pulse-width modulation converter for renewable energy conversion. *International Journal of Circuit Theory and Applications* 2011; **41**(2):168-185.
7. Kassakian JG. High frequency switching and distributed conversion in power electronic systems. *Proceedings of Sixth Conference on Power Electronincs and Motion Control, Budapest, Hungary, 1990*, 1990; 990–994.
8. Perreault D, Kassakian J. Distributed interleaving of paralleled power converters. *Circuits and Systems I: Fundamental Theory and Applications, IEEE Transactions on* 1997; **44**(8):728–734.
9. Huang Y, Tse CK. Circuit theoretic classification of parallel connected dc ndash;dc converters. *Circuits and Systems I: Regular Papers, IEEE Transactions on* 2007; **54**(5):1099–1108.
10. Debbat M, El Aroudi A, Giral R, Martinez-Salamero L. Hopf bifurcation in PWM controlled asymmetrical interleaved dual boost dc-dc converter. *IEEE International Conference on Industrial Technology* 2003; **2**:860–865.
11. Davoudi A, Jatskevich J, Chapman P. Numerical dynamic characterization of peak current-mode-controlled dc-dc converters. *IEEE Transactions on Circuits and Systems-II* 2009; **56**(12):906–910.
12. Zhou G, Xu J. Digital peak current control for switching dc-dc converters with asymmetrical dual-edge modulation. *IEEE Transactions on Circuits and Systems-II* 2009; **56**(11):815-819.
13. Moon YJ, Roh YS, Gong JC, Yoo C. Load-independent current control technique of a single-inductor multiple-output switching dc-dc converter. *IEEE Transactions on Circuits and Systems-II* 2012; **59**(1):50–54.
14. Ma W, Wang M, Liu S, Li S, Yu P. Stabilizing the average-current-mode-controlled boost PFC converter via washout-filter-aided method. *IEEE Transactions on Circuits and Systems-II* 2011; **58**(9):595–599.
15. Iu HHC, Tse CK, Lai YM. Effects of interleaving on the bifurcation behaviour of parallel-connected buck converters. *IEEE International Conference on Industrial Technology* 2002; **2**:1072–1077.
16. Iu HHC, Pjevalica V, Robert B. Implementation of a simple rotating master control scheme for parallel converters. *Power Electronics Specialists Conference, 2004. PESC 04. 2004 IEEE 35th Annual*, vol. 2 2004; 1494–1499.
17. Ishikawa Y, Saito T. Bifurcation of multiple-input parallel dc-dc converters with dynamic winner-take-all switching. *IEEE International Symposium on Circuits and Systems* 2007; 789–792.
18. Iu HHC, Tse CK, Dranga O. Bifurcation in parallel-connected buck converters under current-mode control. *IEEE International Symposium on Circuits and Systems* 2005; **5**:4445–4448.
19. Iu HHC, Zhou Y, Tse CK. Fast-scale instability in a PFC boost converter under average current-mode control. *International Journal of Circuit Theory and Applications* 2003; **31**:611–624.
20. Chan WCY, Tse CK. Bifurcations in current-programmed dc/dc buck switching regulators—conjecturing a universal bifurcation path. *International Journal of Circuit Theory and Applications* 1998; **26**(2):127–145.

21. D'Amico MB, Angulo F, Olivar G, Paolini EE, Moiola JL. Influence of period-doubling bifurcations in the appearance of border collisions for a zad-strategy-controlled buck converter. *International Journal of Circuit Theory and Applications* 2012; **40**(1):77–91.

22. Banerjee S, Verghese GC (eds). *Nonlinear Phenomena in Power Electronics: Attractors, Bifurcations, Chaos, and Nonlinear Control*. IEEE Press: New York, 2001.

23. Tse CK. *Complex Behavior of Switching Power Converters*. CRC Press: Boca Raton, USA, 2003.

24. di Bernardo M, Budd C, Champneys AR, Kowalczyk P. *Piecewise-smooth Dynamical Systems*. Springer-Verlag: London, 2008.

25. El Aroudi A, Benadero L, Toribio E, Machiche S. Quasiperiodicity and chaos in the dc-dc buck-boost converter. *International Journal of Bifurcation and Chaos* 2000; **10**(2):359–371.

26. Mazumder SK, Nayfeh AH, Boroyevich D. Theoretical and experimental investigation of the fast- and slow-scale instabilities of a dc-dc converter. *IEEE Transactions on Power Electronics* 2001; **16**(2):201–216.

27. Giaouris D, Banerjee S, Zahawi B, Pickert V. Control of fast scale bifurcations in power-factor correction converters. *IEEE Transactions on Circuits and Systems-II* 2007; **54**(9):805–809.

28. Wong SC, Wu X, Tse C. Sustained slow-scale oscillation in higher order current-mode controlled converter. *IEEE Transactions on Circuits and Systems-II* 2008; **55**(5):489–493.

29. El Aroudi A, Rodriguez E, Leyva R, Alarcon E. A design-oriented combined approach for bifurcation prediction in switched-mode power converters. *IEEE Transactions on Circuits and Systems–II* 2010; **57**(3):218–222.

30. Iu HHC, Tse CK. Study of low-frequency bifurcation phenomena of a parallel-connected boost converter system via simple averaged models. *IEEE Transactions on Circuits and Systems-I* 2003; **50**(5):679–685.

31. Li M, Tse CK, Iu HHC, Ma X. Unified equivalent modeling for stability analysis of parallel-connected dc/dc converters. *IEEE Transactions on Circuits and Systems-II* 2010; **57**(11):898–902.

32. Iu HHC, Tse CK. Bifurcation behavior in parallel-connected buck converters. *IEEE Transactions on Circuits and Systems-I* 2001; **48**(2):233–240.

33. Zhusubaliyev ZT, Mosekilde E. Torus birth bifurcations in a dc/dc converter. *IEEE Transactions on Circuits and Systems-I* 2006; **53**(8):1839–1850.

34. Zhusubaliyev ZT, Mosekilde E, Maity S, Mohanan S, Banerjee S. Border collision route to quasiperiodicity: Numerical investigation and experimental confirmation. *Chaos* 2006; **16**:023 122 023122(1-11).

35. Zhusubaliyev ZT, Mosekilde E, Yanochkina OO. Torus bifurcation mechanisms in a dc/dc converter with pulse-width modulated control. *IEEE Transactions on Power Electronics* 2011; **26**:1270–1279.

36. Zhusubaliyev ZT, Mosekilde E, Yanochkina OO. Torus bifurcations in multilevel converter systems. *International Journal of Bifurcation and Chaos* 2011; **21**:2343–2356.

37. Giaouris D, Banerjee S, Zahawi B, Pickert V. Stability analysis of the continuous conduction mode buck converter via Filippov's method. *IEEE Transactions on Circuits and Systems I* 2008; **55**(4):1084–1096.

38. Filippov AF. *Differential equations with discontinuous righthand sides*. Kluwer Academic Publishers: Dortrecht, 1988.

39. Aizerman MA, Gantmakher FR. On the stability of periodic motions. *Journal of Applied Mathematics and Mechanics (translated from Russian)* 1958; 1065–1078.

40. Kuznetsov YA. *Elements of Applied Bifurcation Theory*. Springer: New York, USA, 2004.

41. Chen Y, Tse CK, Wong SC, Qiu SS. Interaction of fast-scale and slow-scale bifurcations in current-mode controlled dc/dc converters. *International Journal of Bifurcation and Chaos* 2007; **17**(5):1609–1622.

42. Dankowicz H, Piiroinen P, Nordmark A. Low-velocity impacts of quasiperiodic oscillations. *Chaos Solitons & Fractals* 2002; **14**(2):241–255.

43. Giaouris D, Banerjee S, Imrayed O, Mandal K, Zahawi B, Pickert V. Complex interaction between tori and onset of three-frequency quasi-periodicity in a current mode controlled boost converter. *IEEE Transactions on Circuits and Systems-I* 2012; **59**(1):207–214.

44. Strogatz SH. *Nonlinear Dynamics and Chaos*. Addison-Wesley, 1994 New York.